Applied Catalysis B: Environmental 166–167 (2015) 509–517

Contents lists available at ScienceDirect

Applied Catalysis B: Environmental

journal homepage: www.elsevier.com/locate/apcatb

# Dynamics of $N_2$ and $N_2O$ peaks during and after the regeneration of lean $NO_x$ trap☆

David Mráček[a], Petr Kočí[a,*], Miloš Marek[a], Jae-Soon Choi[b], Josh A. Pihl[b], William P. Partridge[b]

[a] Institute of Chemical Technology, Prague, Department of Chemical Engineering, Technická 5, Prague 166 28, Czech Republic
[b] Fuels, Engines and Emissions Research Center, Oak Ridge National Laboratory, P.O. Box 2008, MS-6472, Oak Ridge, TN 37831, USA

ARTICLE INFO

*Article history:*
Received 17 October 2014
Received in revised form
28 November 2014
Accepted 1 December 2014
Available online 4 December 2014

*Keywords:*
$NO_x$ storage catalyst
$NO_x$ reduction
$N_2O$ formation
$N_2$ formation
Exhaust gas aftertreatment

ABSTRACT

The dynamics and selectivity of $N_2$ and $N_2O$ formation during and after the regeneration of a commercial $NO_x$ storage catalyst containing Pt, Pd, Rh, Ba on Ce/Zr, Mg/Al and Al oxides was studied with high-speed FTIR and SpaciMS analyzers. The lean/rich cycling experiments (60 s/5 s and 60 s/3 s) were performed in the temperature range 200–400 °C, using $H_2$, CO, and $C_3H_6$ individually for the reduction of adsorbed $NO_x$. Isotopically labeled $^{15}NO$ was employed in combination with Ar carrier gas in order to quantify the $N_2$ product by mass spectrometry. $N_2$ and $N_2O$ products were formed concurrently. The primary peaks appeared immediately after the rich-phase inception, and tailed off with breakthrough of the reductant front (accompanied by $NH_3$ product). Secondary $N_2$ and $N_2O$ peaks appeared at the rich-to-lean transition as a result of reactions between surface-deposited reductants/intermediates (CO, HC, $NH_3$, -NCO) and residual stored $NO_x$. At 200–300 °C, up to 30% of $N_2$ and 50% of $N_2O$ products originated from the secondary peaks. The $N_2O/N_2$ selectivity ratio as well as the magnitude of secondary peaks decreased with temperature and duration of the rich phase. Among the three reductants, propene generated secondary $N_2$ peak up to the highest temperature. The primary $N_2$ peak exhibited a broadened shoulder aligned with movement of reduction front from the zone where both $NO_x$ and oxygen were stored to the $NO_x$-free zone where only oxygen storage capacity was saturated. $N_2$ formed in the $NO_x$-free zone originated from reaction of $NH_3$ with stored oxygen, while $N_2O$ formation in this zone was very low.

© 2014 Elsevier B.V. All rights reserved.

## 1. Introduction

$NO_x$ storage and reduction catalyst (NSRC), also known as Lean $NO_x$ trap (LNT), is one of the technologies for aftertreatment of exhaust gas from lean gasoline and diesel engines in automotive applications. It enables $NO_x$ adsorption under lean conditions when the amount of reducing species in the exhaust gas is not high enough to provide a sufficient $NO_x$ reduction. Due to a limited $NO_x$ storage capacity, the catalyst needs to be regenerated periodically by rich pulses containing excess of CO, $H_2$ and hydrocarbons from fuel.

The $NO_x$ adsorption processes taking place under lean conditions are relatively slow. Over last two decades they have been studied extensively and are quite well understood [1–5]. On the other hand, the mechanisms of highly dynamic reduction of stored $NO_x$ during the regeneration pulse are much less explored, particularly under few-seconds time scales relevant to real operation [6] when all processes are highly transient and the catalyst is far from steady state conditions. The regeneration products include $N_2$ (desired final product), desorbed $NO_x$, $NH_3$ and $N_2O$.

When $H_2$ is used as the $NO_x$ reducing agent, $NH_3$ is the main product of $NO_x$ reduction in the fully reduced part of the catalyst. However, at the leading edge of the reduction front $H_2$ initially reacts with the surface-deposited $NO_x$ over incompletely reduced PGM (platinum group metal) sites with a high local $NO_x$:$H_2$ ratio, and $N_2O$ is likely to form under such conditions [7]. As the reduction front travels along the monolith channel, the primary $N_2O$ peak is

☆ Notice: This manuscript has been authored by UT-Battelle, LLC under Contract No. DE-AC05-00OR22725 with the U.S. Department of Energy. The United States Government retains and the publisher, by accepting the article for publication, acknowledges that the United States Government retains a non-exclusive, paid-up, irrevocable, world-wide license to publish or reproduce the published form of this manuscript, or allow others to do so, for United States Government purposes. The Department of Energy will provide public access to these results of federally sponsored research in accordance with the DOE Public Access Plan (http://energy.gov/downloads/doe-public-access-plan).

* Corresponding author. Tel.: +420 22044 3293; fax: +420 22044 4320.
*E-mail addresses:* petr.koci@vscht.cz (P. Kočí), partridgewp@ornl.gov (W.P. Partridge).
*URL:* http://www.vscht.cz/monolith (P. Kočí).

http://dx.doi.org/10.1016/j.apcatb.2014.12.002
0926-3373/© 2014 Elsevier B.V. All rights reserved.

observed at the reactor outlet continuously before breakthrough of the reduction front [8]. The $NH_3$ formed in the already reduced front part of the catalyst is transported by convection downstream into the still oxidized zone, where it reacts with the stored oxygen and $NO_x$ to give $N_2$ and $N_2O$. This leads to a delayed breakthrough of ammonia at the reactor outlet [9–13]. After switch back to the lean conditions, a secondary $N_2O$ peak can be observed at the reactor outlet at low-intermediate temperatures. This secondary peak comes from the reactions of the adsorbed reductants and reduction intermediates with the residual $NO_x$ remaining on the surface after an incomplete regeneration [7]. During the regeneration with $H_2$ in the absence of CO and $CO_2$, the main reduction intermediate is adsorbed $NH_3$. The accumulation of $NH_4NO_3$ is not a major pathway for secondary $N_2O$ formation at low temperatures because most stored $NO_x$ are in the form of nitrites [14]. The secondary peak diminishes with a longer and more complete regeneration that does not leave enough residual $NO_x$ and reduction intermediates on catalyst surface [7].

In the case when CO is used as the reducing agent (or produced *in situ* from $H_2$ and $CO_2$ by reverse water gas shift), the mechanism of stored $NO_x$ reduction proceeds through an isocyanate (-NCO) surface intermediate [15–18] that can further react with NO, $O_2$, stored nitrites/nitrates and $H_2O$ to form $N_2O$, $N_2$ or $NH_3$. Ammonia formed by hydrolysis of -NCO can further react with $NO_x$ stored on the catalyst surface and thus further contribute to the overall $NO_x$ conversion [19]. Despite the relatively fast rate of -NCO hydrolysis a substantial accumulation of isocyanates on the catalyst surface was observed during the rich phase in the presence of water, and it was proposed that the decomposition of isocyanates can be responsible for the secondary $N_2$ and $N_2O$ formation at the transition from rich to lean conditions [6,7,20]. The experimental study [21] demonstrated high selectivity of the -NCO reaction with $O_2$ to molecular nitrogen, therefore the $NO_x$ presence seems to be an important parameter driving the selectivity to $N_2O$ [22]. However, in our recent publication [7] we have shown that the magnitude of the secondary $N_2O$ peak does not depend on the presence of NO in the lean feed after regeneration, and that the secondary $N_2O$ peak (though smaller) can be formed even in the absence of oxygen. Therefore we proposed that the main source of the secondary $N_2O$ peak is the reaction of residual stored $NO_x$ with adsorbed reductants and reduction intermediates remaining on catalyst surface after the short rich phase.

In the case of reduction with hydrocarbons, a wider variety of organic species produced during rich conditions can contribute to the secondary $N_2O$ formation upon return to the lean phase [23]. A parallel, indirect pathway of $NO_x$ reduction by CO and hydrocarbons under rich conditions involves water gas shift and steam reforming reactions where hydrogen formed from CO and hydrocarbons in the presence of water acts as the $NO_x$ reducing agent [24,25].

If hydrocarbons are present in the lean mixture, a limited level of steady-state lean $NO_x$ reduction is achieved in a temperature window around the light-off. Unfortunately, the selectivity of lean $NO_x$ reduction over PGM-based catalysts (DOC, LNT and TWC) is poor and this reaction can lead to additional $N_2O$ emissions during the lean operation period [26].

From the above-discussed observations it is obvious that the global $NO_x$ reduction selectivity depends on many factors, e.g., temperature, spatiotemporal distribution of $NO_x$ storage along the catalyst channel, reductant type, length of the rich period, and also on the actual state of platinum group metals (PGM) [8,24,27].

Even if tailpipe ammonia slip is generally undesired, $NH_3$ is a reactive by-product that can be utilized in further $NO_x$ reduction, e.g., in the case of combined $NO_x$ storage and $NH_3$-SCR catalytic systems [28,29]. In contrast, $N_2O$ is an undesired by-product with low reactivity – although not toxic, it possesses a high global warming potential. Evolution of $NO_x$, $NH_3$ and $N_2O$ can be readily measured with FTIR analyzers, however, the main $N_2$ product dynamics is more difficult to capture in full mixtures and therefore it is usually not followed in detail.

**Table 1**
Inlet gas composition.

| Component | Concentration | |
|---|---|---|
| | Lean | Rich |
| Nitrogen oxide (NO) | 300 ppm | 0 ppm |
| Oxygen ($O_2$) | 10% | 0% |
| Hydrogen ($H_2$) | 0% | 3.4% |
| Carbon monoxide (CO) | 0% | 3.4% |
| Propene ($C_3H_6$) | 0 ppm | 3780 ppm |
| Water ($H_2O$) | 5% | 5% |
| Carbon dioxide ($CO_2$) | 0% | 0% |

In this paper we present the results of an experimental study aiming to further clarify the $NO_x$ regeneration mechanisms over a fully formulated commercial $NO_x$ storage catalyst under practical operating conditions with few seconds long rich phase. The catalyst contains platinum group metals (Pt, Pd, Rh) and Ba, CeZr, MgAl and Al oxides (lean-GDI, BMW 120i, Model Year 2009), which is a reference catalyst within the CLEERS research community [30]. Dynamics and selectivity of $NO_x$ reduction towards all relevant N-products ($N_2$, $N_2O$ and $NH_3$) were measured in dependence on temperature, reductant ($H_2$, CO, $C_3H_6$) and regeneration length relevant to practical application. To achieve that, a novel approach was developed that combines FTIR analysis with SpaciMS experiments using isotopically labeled $^{15}NO$ and Ar as carrier gas. Particular attention was given to the $N_2$ and $N_2O$ double-peak behavior first reported in [6] and further explored in recent studies [7,20]. These studies suggest that a significant part of the $NO_x$ reduction products can actually be formed after the rich-phase end, which is enabled by the reactions of adsorbed reduction intermediates upon transition back to lean conditions. This effect has become a key part of the recently developed technology Di-Air [31,32] that uses high-frequency lean/rich cycling with very short rich pulses.

## 2. Experimental setup

The dynamics of products evolution was examined during lean/rich cycles in a bench flow reactor with synthetic exhaust gases. The lean and rich mixture composition is described in Table 1. The gas hourly space velocity (GHSV) was 30,000 $h^{-1}$ and the tested temperature range was 200–400 °C. Two different regeneration lengths (3 or 5 s) were used while the lean phase length was kept constant (60 s).

The catalyst sample (2.1-cm diameter, 3.8-cm long) was wrapped in Zetex insulation tape and inserted into a horizontal quartz glass tube reactor, which was heated by an electric furnace. Inlet gas mixtures were prepared from pressurized gas cylinders (ultra high purity grade, Air Liquide) and pre-heated before entering the reactor. Precise amounts of the desired gases were dosed through mass flow controllers (Unit Instruments Series 7300, Kinetics Electronics). Water was introduced by a high pressure liquid metering pump (Eldex) to a heated zone, vaporized instantly and added to the simulated exhaust mixture. A rapid switching 4-way valve was used to promptly alternate between the lean and rich gas mixtures [7,27].

First, temporally resolved evolution of products at the reactor outlet was analyzed by a high-speed FTIR gas analyzer (MKS 2030HS) in lean/rich cycling experiments using unlabeled NO and $N_2$ as the carrier gas. The sampled gas was diluted after the reactor outlet to increase the flow-rate through the analyzer and to improve its dynamic response. The internal volume of FTIR measurement cell was ca. 0.2 $dm^3$ and the diluted flow-rate

12 $dm^3$/min, leading to the mean residence time in the analyzer around 1 s. Signal dispersion in the analyzers is a key consideration for interpreting measured data. Low analyzer flow-rate leads to broadening and blending of concentration dynamics during and after regeneration, and obscure their distinct nature; in a limiting case this can cause all product formation to be detected in a single wide peak, dispersed tens of seconds into the subsequent lean phase [26].

The spatiotemporal profiles inside the catalyst channel were then obtained with the in-house developed spatially resolved capillary inlet mass spectrometer (SpaciMS) [33]. In order to enable accurate quantification of produced $N_2$ and $N_2O$ in the SpaciMS experiments, standard $^{14}NO$ was replaced by isotopically labeled $^{15}NO$ and Ar was used as carrier gas. Gas was sampled from different axial locations inside a catalyst channel using a small capillary probe (200-μm outer diameter, 100-μm inner diameter) and fed (through an orifice) into a mass spectrometer for speciation. A relative longitudinal coordinate 0.00–1.00*L* is used to denote location of the probe (0.00*L* corresponds to the inlet, 1.00*L* corresponds to the outlet of the catalyst sample).

To further simplify the quantitative analysis of MS signals, $CO_2$ was excluded from the feed in all experiments (both FTIR and SpaciMS). Although the $CO_2$ parent ion is identified at $m/z$ 44, it contributes also to many other signals (e.g., $m/z$ 16, 22, 28, 45, 46 [34]), particularly at high $CO_2$ levels around several percent. Even if a certain amount of $CO_2$ was formed in the reactor in the case of regeneration by CO and $C_3H_6$, this concentration was still an order of magnitude lower than that usually present in full exhaust mixture. We have shown in our recent paper [7] that $CO_2$ affects the catalyst performance in two ways: (i) decreases the $NO_x$ storage capacity by competitive formation of carbonates on $NO_x$ storage sites, and (ii) inhibits the regeneration with $H_2$ by reverse water gas shift reaction forming carbonyls on PGM sites and eventually gaseous CO. Despite these effects, we believe that the absence of $CO_2$ in our feed gas does not alter the conclusions we reach from this study. Considering the isotopically labeled $^{15}N$, the species of interest were then measured by SpaciMS as follows: $N_2$ at $m/z$ 30, $N_2O$ at $m/z$ 46, and NO at $m/z$ 31.

## 3. Data processing

The processing of spatiotemporal data from SpaciMS experiments involved averaging of three lean/rich cycles obtained after a stationary cycling condition had been achieved to improve the signal/noise ratio and to minimize the errors in local maxima of narrow and sharp peaks where the measurement could become limited by sampling period. The following procedure was then used to convert the MS signals into concentrations.

The total amount of $N_2O$ formed over the cycle was integrated from the FTIR measurements providing the $N_2O$ concentration at the reactor outlet. Correspondingly, the SpaciMS signal of $m/z$ 46 ($N_2O$) at the sample outlet was also integrated. The ratio between those two integrals was then used as a scaling factor for the conversion of $m/z$ 46 into $N_2O$ concentration (constant factor applied to all spatial locations).

The total amount of $N_2$ product was then calculated from the N-atoms balance over the cycle, considering that the sum of formed $N_2$, $N_2O$, $NH_3$ and released $NO_x$ during stationary lean/rich cycles has to be equal to the total amount of $NO_x$ fed to the reactor. For a constant flowrate it is then:

$$2\int_{t_1}^{t_2} y_{N_2}^{out}\,dt = \int_{t_1}^{t_2} y_{NO_x}^{in}\,dt - \int_{t_1}^{t_2} y_{NO_x}^{out}\,dt - 2\int_{t_1}^{t_2} y_{N_2O}^{out}\,dt - \int_{t_1}^{t_2} y_{NH_3}^{out}\,dt, \quad (1)$$

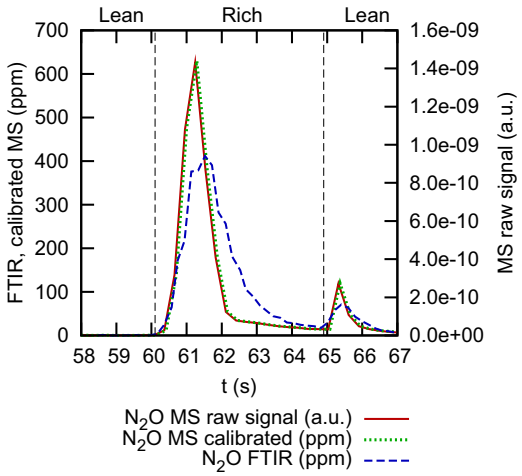


**Fig. 1.** Comparison of the outlet $N_2O$ signals from SpaciMS and FTIR analyzers during 5 s regeneration with $C_3H_6$ at 300 °C.

where $t_1$ is the beginning of the lean phase and $t_2$ is the end of the rich phase (i.e., one complete lean/rich cycle). All integrals on the right hand side of Eq. (1) were evaluated from FTIR measurements, enabling calculation of the integral $N_2$ product amount. The MS signal of $m/z$ 30 ($N_2$) at the sample outlet was also integrated and the ratio between those two integrals was then used as a scaling factor for the conversion of $m/z$ 30 signal into $N_2$ concentration (again, constant factor applied to all spatial locations).

A comparison of the FTIR and SpaciMS measurements (Fig. 1) reveals that the FTIR signal is somewhat more dispersed than that measured by the mass spectrometer. The broadening of peaks reflects a longer residence time of the sampled gas in the measurement cell of the FTIR. Nevertheless, both signals exhibit similar dynamics as well as relative magnitude of primary and secondary peaks. This justifies the use of FTIR measured concentrations for scaling the SpaciMS data as well as compatibility of the experiments with isotopically labeled and unlabeled NO. The two vertical dashed lines in Fig. 1 indicate the transitions between the lean and rich phases. The left dashed line at the earlier time indicates the end of the lean phase and the start of the rich phase; similarly, the right-hand dashed line at the later time indicates the end of the rich phase and the start of the lean phase. The same notation is used in all subsequent figures.

## 4. Results and discussion

### 4.1. Overall $NO_x$ conversion

As it has been discussed in Section 1, the $NO_x$ reduction dynamics, conversion and product selectivity during lean/rich cycles largely depends on the reductant activity. The integral $NO_x$ conversions achieved with $H_2$, CO and $C_3H_6$ are summarized in Fig. 2. It can be seen that almost full conversion is achieved above the "light-off" temperature of each reductant. Pure hydrogen is clearly the most active reductant providing full conversion already at 200 °C. Somewhat lower regeneration efficiency and a higher light-off temperature can be expected for real exhaust operation where $CO_2$ and CO are present, inhibiting the $H_2$ reactions [7,24]. The light-off temperature for CO-rich mixture is between 200 and 250 °C and temperatures above 300 °C are needed for efficient LNT regeneration by $C_3H_6$. This comparison clearly illustrates that the effective $NO_x$ storage capacity of the LNT sample over the studied range of temperatures is high enough to provide complete adsorption of $NO_x$

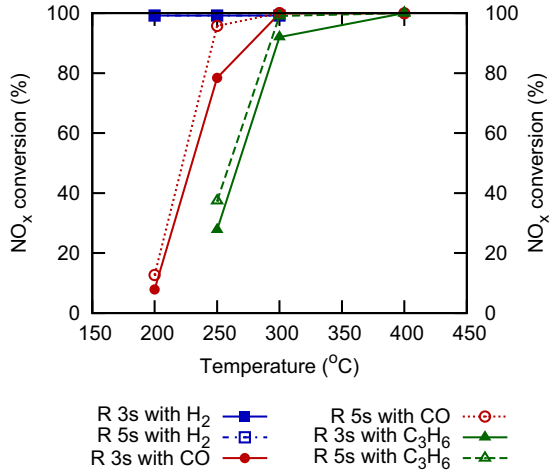


**Fig. 2.** Integral $NO_x$ conversions in lean/rich 60 s/3 s and 60 s/5 s cycles with different reductants.

during the 60-s long lean phase, and any loss of efficiency is caused just by incomplete regeneration during the applied rich phase.

### 4.2. Spatiotemporal $NO_x$ profiles during lean phase

Typical spatiotemporal $NO_x$ profiles in the gas flowing along the monolith channel during the lean/rich cycling are shown in Fig. 3. The situation with an incomplete regeneration is shown in Fig. 3a ($C_3H_6$ at 250 °C). Here $NO_x$ breakthrough at the catalyst outlet (1.00*L*) can be observed during the lean phase, because the adsorption efficiency is limited by a substantial amount of $NO_x$ remaining on the surface from the previous cycles (a consequence of incomplete regenerations). The corresponding spatial profile of the stored $NO_x$ at the end of the lean phase is schematically depicted in Fig. 4a. In contrast, when regeneration is efficient (Fig. 3b, CO at 300 °C), there is no lean $NO_x$ breakthrough even at one half of the catalyst length (0.50*L*). This means that all $NO_x$ is fully adsorbed within the first half of the catalyst (0.00–0.50*L*), most of it in the first quarter (0.00–0.25*L*). The corresponding spatial profile of the stored $NO_x$ at the end of the lean phase is schematically depicted in Fig. 4b.

### 4.3. Outlet dynamics during and after the regeneration

The evolution of key component concentrations in the outlet gas during the 5 s regeneration with the CO-rich mixture at 300 °C can be seen in Fig. 5. The time range shows the very end of lean phase (from 50 to 60 s), the entire rich phase (from 60 to 65 s) and the very beginning of subsequent lean phase (from 65 s). There is no $NO_x$ breakthrough at the end of the lean phase so that a high overall $NO_x$ conversion is achieved at these operating conditions (cf. Fig. 2). Immediately upon the switch to rich conditions, a minor $NO_x$ slip peak appears as a residual of the rapidly released and unreduced $NO_x$. However, the majority of the stored $NO_x$ is reduced to $N_2$ (note the scale of two *y*-axes in Fig. 5). The third peak that appears concurrently with $NO_x$ and $N_2$ is $N_2O$. All these three primary peaks achieve their maxima shortly after the start of regeneration (around 61 s) and then start to decrease. The primary $N_2$ and $N_2O$ peaks then exhibit an interesting feature – a broadening shoulder from ca. 61.5 s to 62.5 s. This will be discussed in more detail later.

Around 2 s after the start of regeneration, $NH_3$ appears at the catalyst outlet together with CO, indicating breakthrough of the reduction front – the PGM and fast OSC (oxygen storage capacity) sites along the entire catalyst have been reduced as well as a large part of the previously stored $NO_x$. From this moment until the end

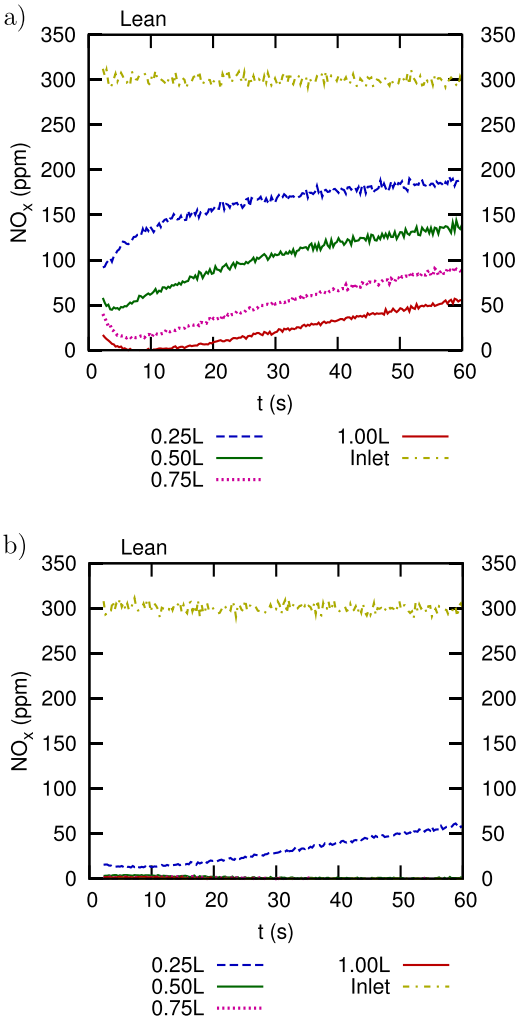


**Fig. 3.** Spatiotemporal $NO_x$ profiles during the lean phase of 60 s/5 s lean/rich cycles. (a) Temperature 250 °C, $C_3H_6$ reductant (low $NO_x$ conversion). (b) Temperature 300 °C, CO reductant (high $NO_x$ conversion).

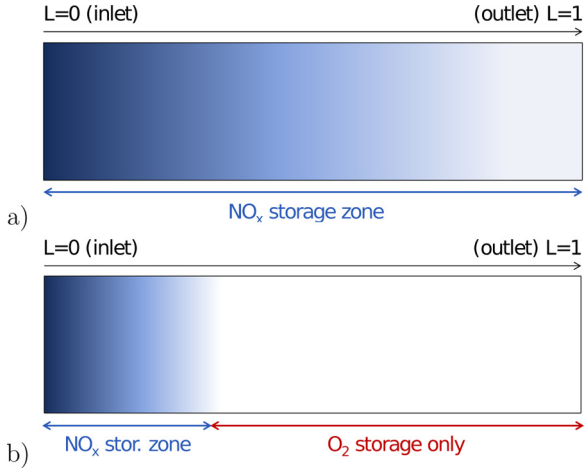


**Fig. 4.** Schematics of stored $NO_x$ profile along the catalyst length at the lean phase end. (a) Low $NO_x$ conversion, cycles with incomplete regeneration. (b) High $NO_x$ conversion, cycles with efficient regeneration.

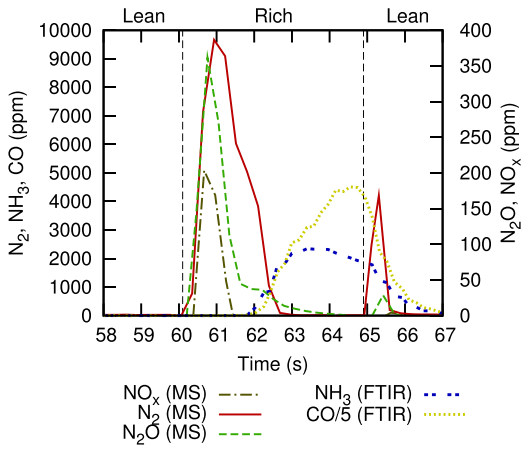


**Fig. 5.** Outlet concentration dynamics of key components during the regeneration with CO-rich mixture at 300 °C.

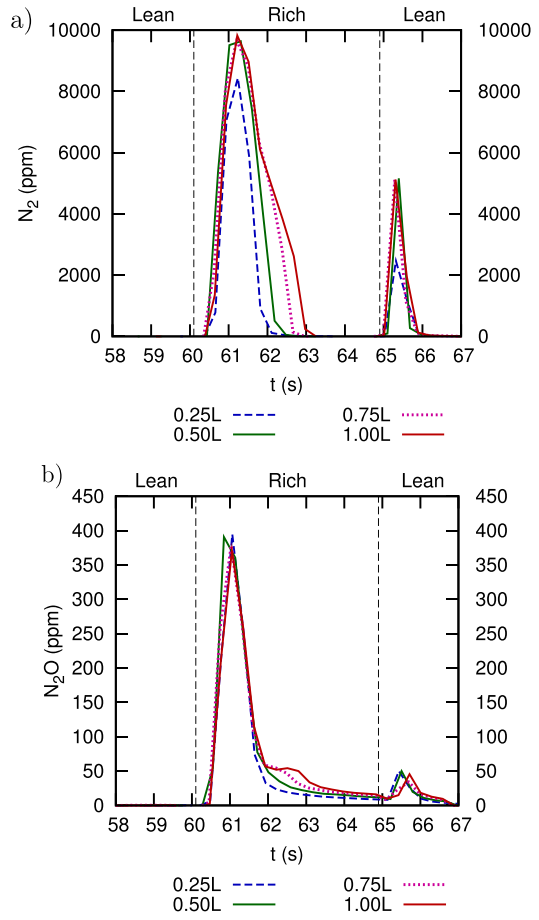


**Fig. 6.** Spatiotemporal concentration profiles of (a) $N_2$ and (b) $N_2O$ products during LNT regeneration. 60 s/5 s lean/rich cycling with CO-rich mixture at 300 °C (high $NO_x$ conversion).

of rich phase, the remaining part of $NO_x$ on the catalyst surface is converted selectively to $NH_3$.

After rich phase termination and the switch back to lean conditions (65 s), $NH_3$ and CO concentrations fall quickly.[1] At the same time, secondary $N_2$ and $N_2O$ peaks appear at the reactor outlet as the products of reactions involving adsorbed reductants and reduction intermediates with residual stored $NO_x$ under increasingly lean conditions. For the CO-rich mixture at this temperature, the most relevant reduction intermediates are isocyanates [6,7,20]. It is known that isocyanates can be hydrolyzed to $NH_3$ (relevant mainly to rich conditions), oxidized readily by $O_2$ with a high selectivity to $N_2$ [21] or react with $NO_x$, the last reaction being the most probable source of $N_2O$ by-product [7]. These reactions are completed within ca. 1–1.5 s so that beyond 66.5 s no N-containing products are detected in the outlet gas, and the catalyst returns fully to the lean $NO_x$ adsorption regime.

### 4.4. Spatiotemporal profiles during and after 5 s rich phase

#### 4.4.1. Efficient reduction above the light-off temperature

Spatiotemporal concentration profiles of the $N_2$ and $N_2O$ products (Fig. 6) provide further details of the regeneration process. It can be seen that the main part of the primary $N_2$ and $N_2O$ peaks in the time interval 60.0–61.5 s is formed in the first quarter of the catalyst (0.25*L*), with no increase in the product concentrations at 0.50–1.00*L*. This is in line with the spatial distribution of stored $NO_x$ prior to the rich phase (cf. Fig. 4), and the fact that both $N_2$ and $N_2O$ are formed during the reduction of stored $NO_x$ at the rich regeneration front over incompletely reduced PGM sites (high O and NO coverage remaining from the lean phase) [8].

A progressively delayed and less intensive evolution of $N_2$ and $N_2O$ products is then observed at the locations 0.50–1.00*L* during 61.5–63 s (Fig. 6), leading to a broadening shoulder of the primary peaks. Two main factors need to be considered when identifying the source of these delayed $N_2$ and $N_2O$ products: first of all, the stored $NO_x$ concentration is negligible in the zone 0.50–1.00*L* (Fig. 4). At the same time (61.5–63 s in Fig. 6), no more $N_2$ and $N_2O$ formation is detected in the first quarter of the catalyst where the $NO_x$ are stored. The reason is that the sole local product of $NO_x$ reduction in that zone is $NH_3$, as could be expected under the fully established rich conditions on the catalyst surface. This is consistent with gradual $NH_3$ and CO breakthrough observed later at the catalyst outlet (Fig. 5). Based collectively on these observations, we can conclude that the source of $N_2$ and $N_2O$ products in the zone 0.50–1.00*L* during 61.5–63.0 s (Fig. 4) is the oxidation of $NH_3$ that has been formed upstream in the first quarter of the catalyst.

It was already demonstrated that the reaction of $NH_3$ with oxygen stored on Ce oxides (oxygen storage sites) is highly selective to $N_2$, while the reaction with stored $NO_x$ significantly increases the selectivity to $N_2O$ [7,27]. This is consistent with the relative magnitude of the product shoulder (61.5–63.0 s) in Fig. 5: The $N_2$ shoulder is two orders of magnitude higher than the $N_2O$ shoulder.

It should be noted that even if all $NO_x$ during the lean phase is trapped within the first quarter of the catalyst, the zone 0.50–1.00*L* is not absolutely free from $NO_x$ because the $NO_x$ slip peak passed to the catalyst outlet at the beginning of the rich phase (cf. Fig. 5) [27]. Partial re-adsorption of this $NO_x$ slip peak is evident from $NO_x$ spatiotemporal concentration profiles shown in Fig. 7. The re-adsorbed $NO_x$ then contributed to minor $N_2O$ formation from 0.50*L* to 1.00*L* during 61.5–63.0 s in Fig. 5 as a by-product of $NH_3 + NO_x$ reaction.

After outlet breakthrough of the reduction front (time 63.0 s in Figs. 5 and 6), $NH_3$ is the sole product of $NO_x$ reduction. Fully rich conditions are established at all locations – OSC is reduced, PGM sites are covered by excess of reductant species and substantial amount of isocyanate intermediates are accumulated on the catalyst surface [7,20]. The reduction of $NO_x$ stored on less accessible Ba sites farther from PGM as well as hydrolysis of isocyanates under these conditions is not completed within the few seconds of remaining rich regeneration.

[1] The measured tails of $NH_3$ and CO peaks are extended by the signal dispersion in FTIR (measurement artifact, cf. the comparison of MS and FTIR signals in Fig. 1).

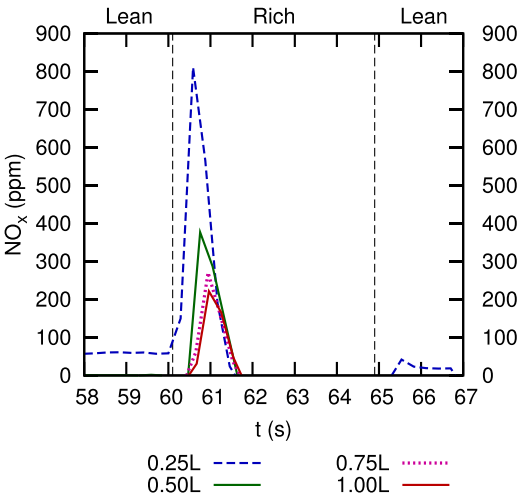


**Fig. 7.** Spatiotemporal concentration profile of $NO_x$ slip peak during LNT regeneration. 60 s/5 s lean/rich cycling with CO-rich mixture at 300 °C (high $NO_x$ conversion).

Therefore, at the moment of switching back to lean conditions (time 65.0 s in Figs. 5 and 6) the catalyst surface is generally covered by a residual amount of unreduced $NO_x$ (relatively low in this case), adsorbed reductants (—CO) and reduction intermediates (-NCO). We can see in Fig. 6 that the reactions of these species under increasingly lean conditions lead to formation of secondary $N_2$ and $N_2O$ peaks mainly in the first quarter of the catalyst (0.25*L*). This spatial distribution is again in line with the fact that mostly the first quarter of the catalyst is used for $NO_x$ storage under these cycling conditions (Figs. 3b and 4b) so that the highest surface concentration of $NO_x$ reduction intermediates is produced here during the rich phase. Qualitatively similar spatiotemporal patterns were observed with all reductants in high conversion mode (above their light-off temperature, cf. Fig. 2).

### 4.4.2. *Inefficient reduction around the light-off temperature*

A different type of product concentration profiles, typical for less active reductant and/or lower temperatures around the rich regeneration light-off, is shown in Fig. 8 (reduction by $C_3H_6$ at 250 °C). Before interpreting the results, let us remind that under these operating conditions the $NO_x$ conversion is relatively low (Fig. 2) and $NO_x$ breaks through during the lean phase (Fig. 3a) so that the $NO_x$ storage zone covers entire catalyst length, even if $NO_x$ is still primarily stored in the front half of the catalyst (Fig. 4a).

When regeneration begins (time 60 s in Fig. 8), $N_2$ and by-product $N_2O$ are formed initially in the front quarter of the catalyst (0.25*L*) but with a small delay also at further locations (0.50–1.00*L*) so that both $N_2$ and $N_2O$ primary peaks grow along the entire catalyst length. Such a gradual build-up of products is in line with the profile of the stored $NO_x$ prior to the regeneration. The progressive delay in product formation in downstream zones correlates with the movement of $C_3H_6$ reductant front towards the outlet, which is relatively fast under these conditions (low temperature, low effective oxygen storage capacity, slow reactions leading to incomplete $C_3H_6$ consumption).

After the $N_2$ and $N_2O$ primary peaks reach their maxima (time 61.5 s in Fig. 8), the product formation rates decrease but still remain relatively high in comparison with the peak values. The $N_2$ and $N_2O$ production continues along the entire catalyst length until the end of the rich phase. This indicates a kinetically controlled regeneration regime, i.e., the product formation is not locally limited by the presence of stored $NO_x$ nor the availability of the reductant. The $NO_x$ reduction rate correlates with the magnitude of the primary $N_2$ peak (main product) and it is obviously much

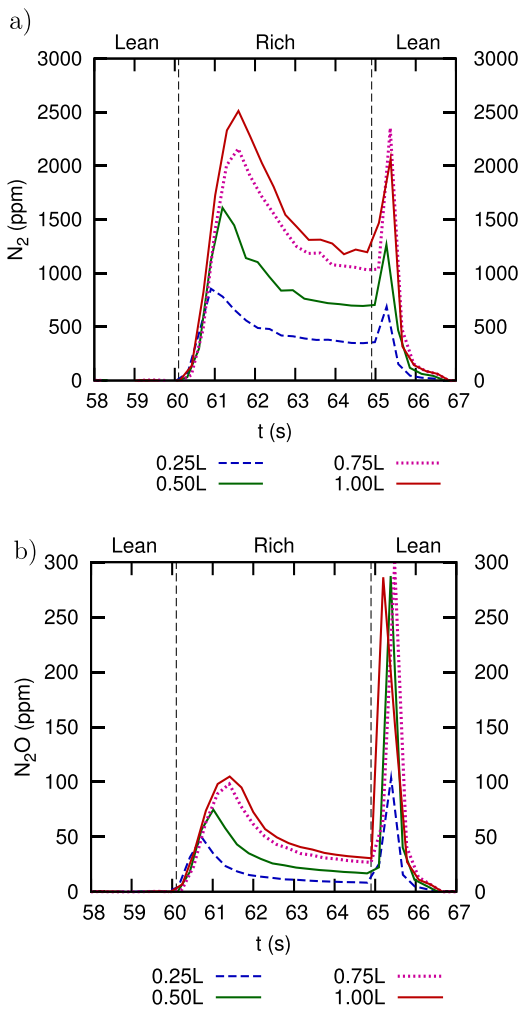


**Fig. 8.** Spatiotemporal concentration profiles of (a) $N_2$ and (b) $N_2O$ products during LNT regeneration. 60 s/5 s lean/rich cycling with $C_3H_6$-rich mixture at 250 °C (low $NO_x$ conversion).

lower than with CO at 300 °C (Fig. 6). The $NO_x$ reduction rate with $C_3H_6$ at 250 °C is also much lower than the corresponding release rate of stored $NO_x$ which leads to a significant rich-phase $NO_x$ slip peak under these conditions (Fig. 9).

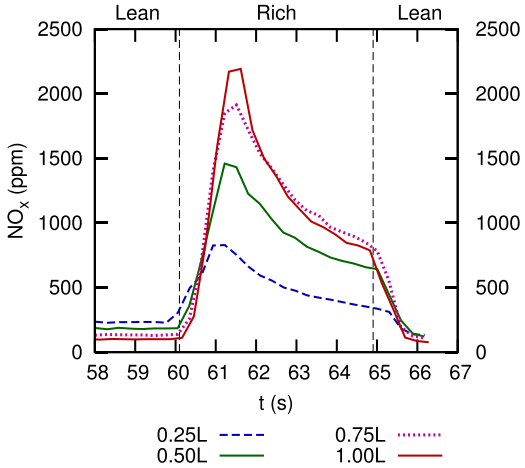


**Fig. 9.** Spatiotemporal concentration profile of $NO_x$ slip peak during LNT regeneration. Lean/rich cycling 60 s/5 s with $C_3H_6$-rich mixture at 250 °C (low $NO_x$ conversion).

Due to low $NO_x$ reduction rate during the $C_3H_6$-rich regeneration at 250 °C, the residual $NO_x$ coverage at the end of the rich phase is still quite high along the entire catalyst length. Furthermore, the catalyst surface is covered by adsorbed reductant ($-C_3H_6$) and reduction intermediates specific for hydrocarbons (not isocyanates). Even if there is no general agreement about the exact structure of these hydrocarbon-related intermediates [23,31], it can be concluded that their reactions after the switch back to lean conditions lead to the formation of secondary $N_2$ and $N_2O$ peaks (time 65.0–67.0 s in Fig. 8).

This behavior is qualitatively similar to the CO-rich mixture (Fig. 6) where isocyanates were key intermediates. Because in this case (Fig. 8) the amount of residual unreduced $NO_x$ is much higher and the lower temperature allows more reductant-related species to accumulate on the surface, the magnitude of the secondary peak is comparable ($N_2$, Fig. 8a) or even significantly higher ($N_2O$, Fig. 8b) than that of primary one. This is further promoted by the fact that the reactions under rich conditions become self-inhibited by the reductant excess (PGM sites blocking), while under lean conditions the reactions accelerate because the PGM sites are freed from excessively high reductant coverage by reactions with oxygen [35]. However, this peak $NO_x$ reduction rate is only transient and falls down again within one second (65.0–66.0 s in Fig. 8) as all the adsorbed reductant/intermediate species are oxidized and there is no more driving force for $NO_x$ reduction.

### 4.5. Contribution of secondary peaks to $N_2$ and $N_2O$ formation

The relative contribution of secondary peaks to the overall $N_2$ or $N_2O$ product formed is dependent on the operating conditions summarized in Fig. 10. It can be seen that the importance of both $N_2$ and $N_2O$ secondary peaks generally decrease with temperature, with $N_2O$ exhibiting steeper dependence than $N_2$. For each reductant, the largest secondary peaks are generally observed at the regeneration light-off temperature (compare with $NO_x$ conversions in Fig. 2). At the light-off temperature, secondary peaks of $N_2O$ represent up to 50% of total $N_2O$ emissions, while the contribution of secondary $N_2$ peaks to overall $N_2$ formation is around 30% for the examined lean/rich timings. However, the contribution of secondary peaks to $N_2O$ formation diminishes relatively fast with the increasing temperature, while secondary $N_2$ peaks decrease more slowly, indicating a change in the product selectivity.

The results in Fig. 10 also show that relative contribution of both the $N_2O$ and $N_2$ secondary peaks increase with the decreasing rich phase length, and this trend holds in the entire examined temperature range. The differences in secondary $N_2$ formation are considerable up to highest temperatures, while for $N_2O$ they become relatively small above the light-off temperature of a given reductant. The dependences on temperature and rich phase length are in line with the previously discussed mechanism of secondary peaks formation – lower temperature and shorter rich phase favor high coverages of both residual unreduced $NO_x$ and adsorbed reductant intermediates.

### 4.6. Spatiotemporal profiles during and after 3 s rich phase

An example of the measured spatiotemporal concentration profiles for the shorter rich phase (3 s) is given in Fig. 11. In comparison with the corresponding profiles at the same temperature and reductant but with a longer rich phase (5 s in Fig. 6), it can be seen that the first three seconds of regeneration (60–63 s) are similar. Only minor differences can be identified for the 3 s rich phase in Fig. 11: slightly slower movement of the reduction front and thus more $N_2$ formed at 0.25–0.50*L*, and a somewhat higher primary $N_2O$ peak. These minor differences indicate a bit higher amount of

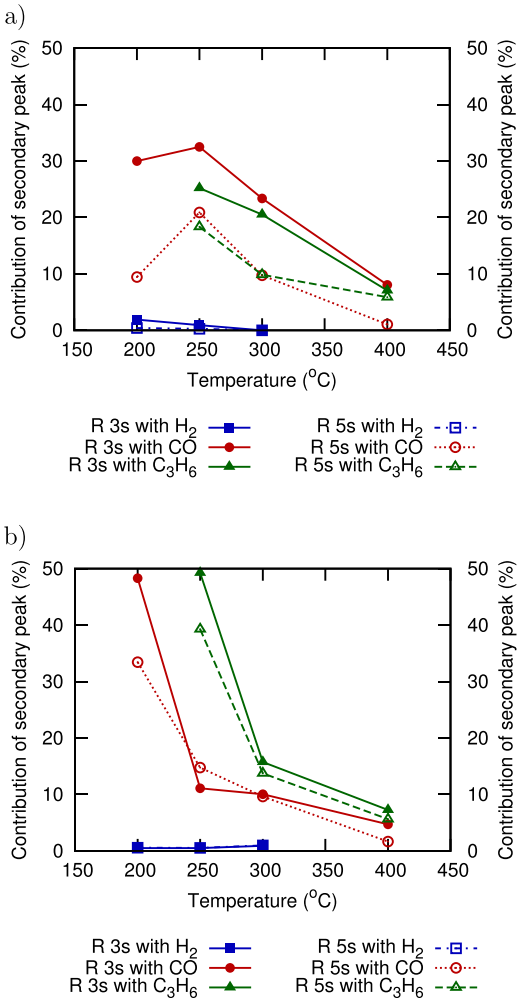


**Fig. 10.** Relative contribution of secondary peak to overall yield of a product depending on operating conditions. a) $N_2$ product, b) $N_2O$ product.

$NO_x$ stored on catalyst surface in the first half of catalyst length as a result of previous less complete regenerations. This is confirmed by the corresponding spatiotemporal $NO_x$ concentration profile during the lean phase (Fig. 12) showing a higher $NO_x$ breakthrough at 0.25*L* than was observed in the case of 5 s regeneration (Fig. 3b). Nevertheless, the $NO_x$ capture is still complete at 0.50*L* so that a high $NO_x$ conversion is maintained also with the shorter regeneration.

Indeed, the main difference between the dynamics of 3 s regeneration (Fig. 11) and 5 s regeneration (Fig. 6) is a higher magnitude of the secondary peaks after the shorter regeneration. The magnitude of the $N_2$ secondary peak appears to be more sensitive to rich phase length than that of $N_2O$. In the case of 3 s regeneration, the rich phase ended just at the beginning of $NH_3$ and CO breakthrough (compare with time 63 s in Fig. 5) and the remaining surface $NO_x$ and accumulated isocyanates were converted under increasingly lean conditions mostly to $N_2$ instead of $NH_3$ that would be the main product under continuing rich conditions (c.f. Fig. 5).

### 4.7. $N_2O$ formation trends

The fraction of $N_2O$ product in the sum of $N_2$ and $N_2O$ (indicating the selectivity of $NO_x$ reduction to products excluding $NH_3$) is shown in Fig. 13. This fraction was calculated separately for primary and secondary peaks. At the rich regeneration light-off temperature (200 °C for CO, 250 °C for $C_3H_6$) the fraction of $N_2O$ in the

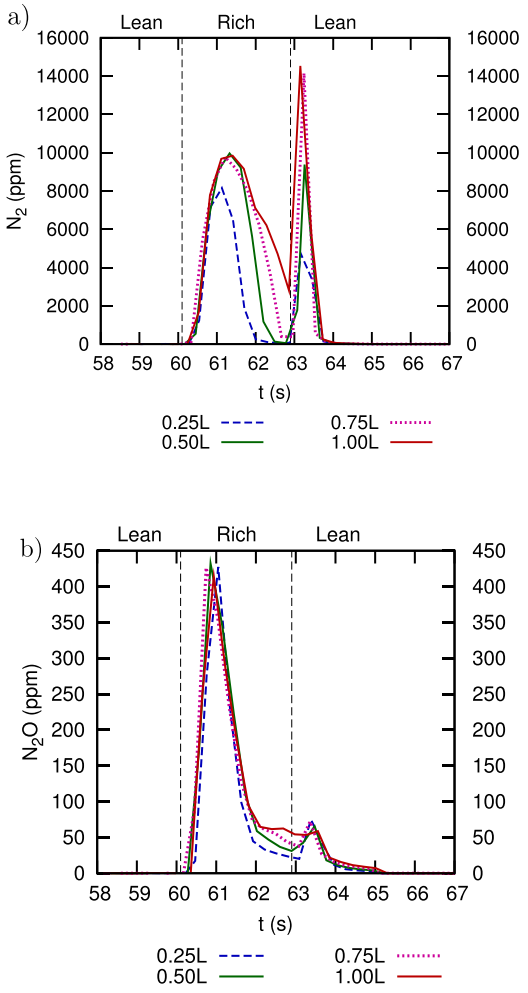


**Fig. 11.** Spatiotemporal concentration profiles of (a) $N_2$ and (b) $N_2O$ products during LNT regeneration. 60 s/3 s lean/rich cycling with CO-rich mixture at 300 °C (high $NO_x$ conversion, shorter regeneration).

secondary peak is significantly higher than in the primary peak, while at higher temperatures the $N_2O$ fractions in both peaks are similar. The increased $N_2O$ selectivity in secondary peaks around the light-off temperature is promoted by high residual coverage

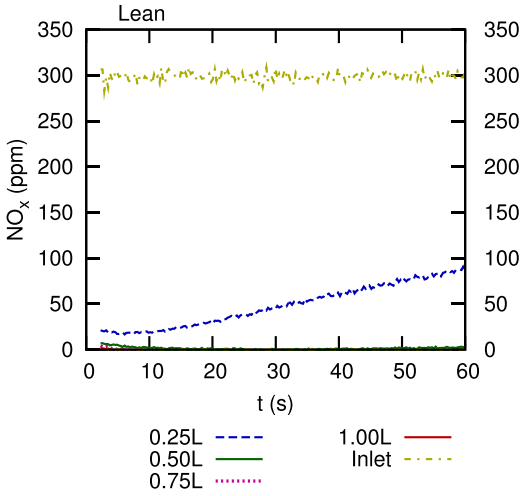


**Fig. 12.** Spatiotemporal $NO_x$ profiles during the lean phase of 60 s/3 s lean/rich cycles with CO-rich mixture at 300 °C (high $NO_x$ conversion, shorter regeneration).

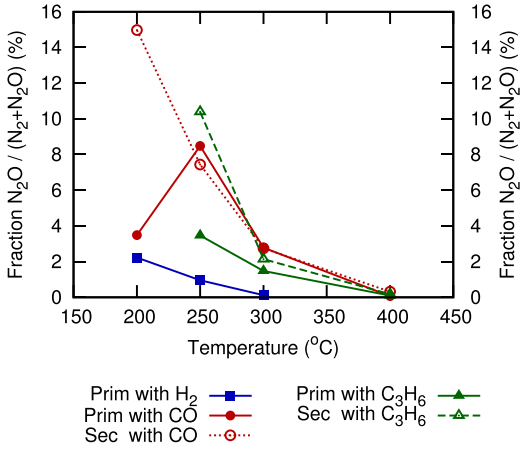


**Fig. 13.** Fraction of $N_2O$ product in the sum of $N_2$ and $N_2O$ formed in primary and secondary peaks during lean/rich cycling 60 s/5 s.

of stored $NO_x$ as well as by gas-phase $NO_x$ slip due to incomplete regeneration during rich phase – a high $NO_x$-to-reductant ratio generally favors $N_2O$ formation. At higher temperatures, the $NO_x$ reduction during rich phase is much more effective so both residual coverage of stored $NO_x$ and gas-phase $NO_x$ slip decrease. At 400 °C the $N_2O$ formation in both primary and secondary peaks is further suppressed by increasing NO dissociation rate on PGM sites and fast interactions with reductants (preventing $N_2O$ formation) as well as by an increasing rate of $N_2O$ decomposition, so that the $N_2O$ selectivity generally reaches negligible values for any reductant used.

## 5. Conclusions

The reported spatiotemporal concentration patterns of $NO_x$ and $NO_x$ reduction products during and after LNT regeneration enabled development of a general reaction mechanism leading to the formation of secondary $N_2$ and $N_2O$ peaks. The results collectively suggest that the secondary peaks are formed by the reactions of adsorbed reductants and reduction intermediates with residual stored $NO_x$. Even if the exact nature of the adsorbed reduction intermediates may differ with temperature and the rich mixture composition (e.g., adsorbed $NH_3$ at the lowest temperature during reduction with hydrogen, isocyanates during reduction with CO, and hydrocarbon-related intermediates with $C_3H_6$), this basic principle seems to hold over the entire range of operating conditions. Lower temperatures and shorter rich phases favor high coverages of both residual stored $NO_x$ and the reduction intermediates that together lead to formation of large secondary peaks upon the transient back to lean conditions. This interpretation seems to be applicable also to different LNT catalyst formulations and gas mixture compositions where similar $N_2O$ and $N_2$ outlet dynamics were reported [6,20].

During conventional lean/rich cycling using a few seconds long rich phase, these secondary peaks are responsible for a significant part of $N_2$ and $N_2O$ products formed at lower and intermediate temperatures (up to 30% and 50%, respectively). With increasing temperature the relative importance of secondary peaks decrease due to decreasing amounts of adsorbed reductant intermediates as well as low residual coverage of stored $NO_x$, however, it is quite probable that with one order of magnitude shorter regeneration times and rapid lean/rich cycling strategy [31] the mechanisms for secondary peaks formation can still play an important role up to the highest temperatures.

## Acknowledgements

This work has been financially supported by the Czech Ministry of Education (Project LH 12086) and the US Department of Energy (DOE) Vehicle Technologies Office (program managers: Gurpreet Singh, Ken Howden and Leo Breton). The co-authors would like to thank Dr. Mi-Young Kim of the ORNL Fuels, Engines and Emissions Research Center for her contributions to the experimental catalyst work.

## References

[1] W.S. Epling, L.E. Campbell, A. Yezerets, N.W. Currier, J.E. Parks, Overview of the fundamental reactions and degradation mechanisms of $NO_x$ storage/reduction catalysts, Catal. Rev. Sci. Eng. 46 (2004) 163–245.
[2] I. Nova, L. Castoldi, L. Lietti, E. Tronconi, P. Forzatti, E. Prinetto, G. Ghiotti, $NO_x$ adsorption study over Pt–Ba/alumina catalysts: FT-IR and pulse experiments, J. Catal. 222 (2004) 377–388.
[3] L. Castoldi, I. Nova, L. Lietti, P. Forzatti, Study of the effect of Ba loading for catalytic activity of Pt–Ba/$Al_2O_3$ model catalysts, Catal. Today 96 (2004) 43–52.
[4] E. Fridell, M. Skoglundh, B. Westerberg, S. Johansson, G. Smedler, $NO_x$ storage in barium-containing catalysts, J. Catal. 183 (1999) 196–209.
[5] F. Rodrigues, L. Juste, C. Potvin, J.F. Tempere, G. Blanchard, G. Djega-Mariadassou, $NO_x$ storage on barium-containing three-way catalyst in the presence of $CO_2$, Catal. Lett. 72 (2001) 59–64.
[6] J.P. Breen, R. Burch, C. Fontaine-Gautrelet, C. Hardacre, C. Rioche, Insight into the key aspects of the regeneration process in the $NO_x$ storage reduction (NSR) reaction probed using fast transient kinetics coupled with isotopically labelled (NO)-N-15 over Pt and Rh-containing Ba/$\gamma$-$Al_2O_3$ catalysts, Appl. Catal. B: Environ. 81 (2008) 150–159.
[7] Š. Bártová, P. Kočí, D. Mráček, M. Marek, J.A. Pihl, J.-S. Choi, T.J. Toops, W.P. Partridge, New insights on $N_2O$ formation pathways during lean/rich cycling of a commercial lean $NO_x$ trap catalyst, Catal. Today 231 (2014) 145–154.
[8] P. Kočí, Š. Bártová, D. Mráček, M. Marek, J.-S. Choi, M.-Y. Kim, J.A. Pihl, W.P. Partridge, Effective model for prediction of $N_2O$ formation during the regeneration of $NO_x$ storage catalyst, Top. Catal. 56 (2013) 118–124.
[9] L. Cumaranatunge, S.S. Mulla, A. Yezerets, N.W. Currier, W.N. Delgas, F.J. Ribeiro, Ammonia is a hydrogen carrier in the regeneration of Pt/BaO/$Al_2O_3$ $NO_x$ traps with $H_2$, J. Catal. 246 (2007) 29–34.
[10] R.D. Clayton, M.P. Harold, V. Balakotaiah, $NO_x$ storage and reduction with $H_2$ on Pt/BaO/$\gamma$-$Al_2O_3$) monolith: spatio-temporal resolution of product distribution, Appl. Catal. B: Environ. 84 (2008) 616–630.
[11] A. Lindholm, N.W. Currier, J. Li, A. Yezerets, L. Olsson, Detailed kinetic modeling of $NO_x$ storage and reduction with hydrogen as the reducing agent and in the presence of $CO_2$ and $H_2O$ over a Pt/Ba/Al catalyst, J. Catal. 258 (2008) 273–288.
[12] P. Kočí, F. Plát, J. Štěpánek, M. Kubíček, M. Marek, Dynamics and selectivity of $NO_x$ reduction in $NO_x$ storage catalytic monolith, Catal. Today 137 (2008) 253–260.
[13] W.P. Partridge, J.-S. Choi, $NH_3$ formation and utilization in regeneration of Pt/Ba/$Al_2O_3$ $NO_x$ storage–reduction catalyst with $H_2$, Appl. Catal. B: Environ. 91 (2009) 144–151.
[14] J.H. Kwak, D.H. Mei, C.W. Yi, D.H. Kim, C.H.F. Peden, L.F. Allard, J. Szanyi, Understanding the nature of surface nitrates in BaO/gamma-$\gamma$-$Al_2O_3$ $NO_x$ storage materials: a combined experimental and theoretical study, J. Catal. 261 (2009) 17–22.
[15] Y. Ji, T.J. Toops, M. Crocker, Isocyanate formation and reactivity on a Ba-based LNT catalyst studied by DRIFTS, Appl. Catal. B: Environ. 140 (2013) 265–275.
[16] I. Nova, L. Lietti, P. Forzatti, F. Frola, F. Prinetto, G. Ghiotti, Reaction pathways in the reduction of $NO_x$ species by CO over Pt-Ba/$\gamma$-$Al_2O_3$: lean $NO_x$ trap catalytic systems, Top. Catal. 52 (2009) 1757–1761.
[17] J.-Y. Luo, W.S. Epling, New insights into the promoting effect of $H_2O$ on a model Pt/Ba/$\gamma$-$Al_2O_3$ NSR catalyst, Appl. Catal. B: Environ. 97 (2010) 236–247.
[18] C.D. DiGiulio, V.G. Komvokis, M.D. Amiridis, In situ FTIR investigation of the role of surface isocyanates in the reduction of $NO_x$ by CO and $C_3H_6$ over model Pt/BaO/$\gamma$-$Al_2O_3$ and Rh/BaO/$\gamma$-$Al_2O_3$ $NO_x$ storage and reduction (NSR) catalysts, Catal. Today 184 (2012) 8–19.
[19] I. Nova, L. Lietti, P. Forzatti, F. Prinetto, G. Ghiotti, Experimental investigation of the reduction of $NO_x$ species by CO and $H_2$ over Pt-Ba/$Al_2O_3$ lean $NO_x$ trap systems, Catal. Today 151 (2010) 330–337.
[20] S. Chansai, R. Burch, C. Hardacre, S. Naito, Origin of double dinitrogen release feature during fast switching between lean and rich cycles for $NO_x$ storage reduction catalysts, J. Catal. 317 (2014) 91–98.
[21] T. Lesage, C. Verrier, P. Bazin, J. Saussey, M. Daturi, Studying the $NO_x$-trap mechanism over a Pt–Rh/Ba/$Al_2O_3$ catalyst by operando FT-IR spectroscopy, Phys. Chem. Chem. Phys. 5 (2003) 4435–4440.
[22] L. Castoldi, L. Lietti, L. Righini, P. Forzatti, S. Morandi, G. Ghiotti, FTIR and transient reactivity experiments of the reduction by $H_2$, CO and HCs of $NO_x$ stored over Pt–Ba/$Al_2O_3$ LNTs, Top. Catal. 56 (2013) 193–200.
[23] E. Joubert, X. Courtois, P. Marecot, C. Canaff, D. Duprez, The chemistry of De$NO_x$ reactions over Pt/$Al_2O_3$: the oxime route to $N_2$ or $N_2O$, J. Catal. 243 (2006) 252–262.
[24] P. Kočí, F. Plát, J. Štěpánek, Š. Bártová, M. Marek, M. Kubíček, V. Schmeisser, D. Chatterjee, M. Weibel, Global kinetic model for the regeneration of $NO_x$ storage catalyst with CO, $H_2$ and $C_3H_6$ in the presence of $CO_2$ and $H_2O$, Catal. Today 147S (2009) 257–264.
[25] P.R. Dasari, R. Muncrief, M.P. Harold, Elucidating $NH_3$ formation during $NO_x$ reduction by CO on Pt–BaO/$Al_2O_3$ in excess water, Catal. Today 184 (2012) 43–53.
[26] L. Masdrag, X. Courtois, F. Can, D. Duprez, Effect of reducing agent ($C_3H_6$, CO, $H_2$) on the $NO_x$ conversion and selectivity during representative lean/rich cycles over monometallic platinum-based NSR catalysts: influence of the support formulation, Appl. Catal. B: Environ. 146 (2014) 12–23.
[27] J.-S. Choi, W.P. Partridge, J.A. Pihl, M.-Y. Kim, P. Kočí, C.S. Daw, Spatiotemporal distribution of $NO_x$ storage and impact on $NH_3$ and $N_2O$ selectivities during lean/rich cycling of a Ba-based lean $NO_x$ trap catalyst, Catal. Today 184 (2012) 20–26.
[28] D. Chatterjee, P. Kočí, V. Schmeißer, M. Marek, M. Weibel, B. Krutzsch, Modelling of a combined $NO_x$ storage and $NH_3$-SCR catalytic system for diesel exhaust gas aftertreatment, Catal. Today 151 (2010) 395–409.
[29] Y. Liu, M.P. Harold, D. Luss, Coupled $NO_x$ storage and reduction and selective catalytic reduction using dual-layer monolithic catalysts, Appl. Catal. B: Environ. 121 (2012) 239–251.
[30] CLEERS web pages, http://www.cleers.org (accessed 2014).
[31] Y. Bisaiji, K. Yoshida, M. Inoue, K. Umemoto, Development of di-air: a new diesel deNOx system by adsorbed intermediate reductants, SAE Int. J. Fuels Lubr. 5 (1) (2012) 380–388, http://dx.doi.org/10.4271/2011-01-2089.
[32] C.C.Y. Perng, V.G. Easterling, M.P. Harold, Fast lean-rich cycling for enhanced $NO_x$ conversion on storage and reduction catalysts, Catal. Today 231 (2014) 125–134.
[33] W.P. Partridge, J.M.E. Storey, S.A. Lewis, R.W. Smithwick, G.L. DeVault, M.J. Cunningham, N.W. Currier, T.M. Yonushonis, Time-Resolved Measurements of Emission Transients by Mass Spectrometry, SAE Technical Paper 2000-01-2952, 2000.
[34] NIST web pages, http://webbook.nist.gov (accessed 2014).
[35] J.-S. Choi, W.P. Partridge, C.S. Daw, Spatially resolved in situ measurements of transient species breakthrough during cyclic, low-temperature regeneration of a monolithic Pt/K/$Al_2O_3$ $NO_x$ storage–reduction catalyst, Appl. Catal. A 293 (2005) 24–40.